Progress in Propulsion Physics **2** (2011) 655-674

WALL PRESSURE AND THRUST OF A DUAL BELL NOZZLE IN A COLD GAS FACILITY

P. Reijasse[1], D. Coponet[1], J.-M. Luyssen[1], V. Bar[2], S. Palerm[2], J. Oswald[2], F. Amouroux[2], J.-C. Robinet[3], and P. Kuszla[3]

[1]ONERA
Meudon 92190, France
[2]CNES
Evry 91023, France
[3]ENSAM
Paris 75000, France

A dual-bell nozzle has been tested in the ONERA-R2Ch wind tunnel within the CNES PERSEUS program. The wall pressure distributions and the thrust for the two flow regimes have been characterized in the nozzle pressure ratio (NPR) range from 51 up to 597. A hysteresis on the transition NPR between the two flow regimes has been observed according to the evolution of NPR. The duration for the switch between the two flow regimes is less than 10 ms. The hysteresis of about 20% on the NPR has also a direct effect on the thrust. The total thrust of the dual-bell nozzle becomes higher than the thrust of the isolated base nozzle without extension for NPR > 1500. The hysteresis phenomenon has been modeled with the use of supersonic separation criteria and by making the assumption that incipient separation occurs immediately after the transition for increasing NPRs, while effective separation occurs just before the transition for decreasing NPRs.

NOMENCLATURE

A_S	exit section
F	thrust
$\overline{F}$	thrust normalized by the thrust at the throat
J	junction
L	nozzle length
M	Mach number
NPR	nozzle pressure ratio (p_t/p_a)

Article available at http://www.eucass-proceedings.eu or http://dx.doi.org/10.1051/eucass/201102655

p	pressure
R	radius
Σ_j	inviscid nozzle jet frontier

Subscripts

1	base nozzle
2	nozzle extension
a	ambient
DB	dual bell
crit	critical (for NPR)
dec	decreasing (for NPR)
id	ideal (for a nozzle)
inc	increasing (for NPR)
t	total (for total pressure)
th	throat
tr	transition

1 INTRODUCTION

Within the PERSEUS program [1] driven by CNES, the possibility is studied to equip a nanosatellite launcher with a dual-bell nozzle. In order to better understand the aerodynamics of this nozzle concept, a cold gas experimental study has been undertaken in the ONERA-R2Ch wind tunnel in 2009. The design method of the dual-bell contour is presented. The wall pressure measurements and the thrust measurements are discussed. First, Reynolds-averaged Navier–Stokes (RANS) computations have been realized.

The dual-bell nozzle is an autoadaptive concept, first proposed in 1949 [2], relying on the altitude compensation. This concept uses a two-section nozzle (Fig. 1). The first part of the divergent section is the base nozzle. The second part is the nozzle extension. At the junction between the two sections, there exists a discontinuity of wall slope (or wall inflection).

In a dual-bell nozzle, two flow regimes exist depending on the nozzle pressure ratio (NPR) relatively to a critical value $\mathrm{NPR}_{\mathrm{crit}}$. The nozzle pressure ratio is expressed as the ratio of the chamber pressure (or total pressure) over the ambient external pressure, $\mathrm{NPR} = p_{\mathrm{t}}/p_{\mathrm{a}}$. During flight, as the chamber pressure of the engine is usually constant, the NPR is continuously increasing during the ascent of rocket.

The sea-level flow regime (Fig. 2*a*) occurs when $\mathrm{NPR} < \mathrm{NPR}_{\mathrm{crit}}$ at the lowest altitudes. The base nozzle is running in a full-flowing regime and the nozzle jet (Σ_j) separates at the junction J between the two sections. A typical

arates at the nozzle lip E. The intensity of the shock issuing from the nozzle lip is equal to p_a/p_2 where p_2 is the wall pressure of the nozzle extension in the attached boundary layer zone. As long as the pressure p_a remains higher than the pressure p_2, the nozzle extension will be a source of drag. Thus it is crucial to determine the critical value $\mathrm{NPR}_{\mathrm{crit}}$ in order to evaluate the thrust losses due to the drag produced by the nozzle extension.

2 SHORT BIBLIOGRAPHICAL SURVEY

The dual-bell nozzle concept has gained renewed interest at the end of 1990s and early 2000s as a possibility to equip the engine of future space transport launch vehicles. In 2003, the Kakuda Space Center of the Japanese agency JAXA considered this nozzle concept has prospects of being used for high-performance engines of reusable space vehicles [3]. The dual-bell concept was under investigation in 2002 as a potential upgrade path for current launch vehicles by Boeing Rocketdyne [4]; the area ratios of the presented dual-bell divergent were $\Sigma_1 \approx 25$ and $\Sigma_{\mathrm{DB}} \approx 150$ and the lengths were respectively $L_1/R_{\mathrm{th}} \approx 6$ and ≈ 16.6. In 2002, European industry and CNES agency also envisaged the dual-bell concept as a good candidate for improving the nozzle performances of the Vulcain rocket engine family [5]; this possibility was the conclusion of specific research efforts conducted within the frame of the joint cooperation FSCD program between Germany (ASTRIUM, DLR), Sweden (VOLVO Aero, SNSB, FOI), and France (CNES, SNECMA, ONERA) with active contribution of ESTEC.

Different design aspects for wall inflection and nozzle extension were discussed in the U.S. NASA study [6] and also in German analytical and experimental studies [7–9] with due regard for the dependence of transition behavior from the sea level to altitude operation on the type of nozzle extension. Several conclusions were derived from these studies. Two different types of nozzle extensions, the constant-pressure extension and the overturned extension [6, 7], might offer more rapid flow transition. The losses caused by wall inflection were shown to have the same order of magnitude as the divergence loss of the base nozzle. The application of commonly used separation criteria derived from conventional nozzles gave reasonable results when applied to dual-bell nozzles [7]. The time needed for the transition and the side loads induced by the transition were also examined [8]. Typical timescales needed for the transition were less than 10 ms for both constant-pressure and overturned pressure contours. For both types of nozzle extensions, a strong hysteresis was observed with respect to the transition nozzle pressure ratio ($\mathrm{NPR}_{\mathrm{tr}}$) with a higher value for the startup. This hysteresis effect was found to be an obstacle for a potential pulsation between the two dual-bell flow regimes [8]. The effect of the nozzle extension length on the NPR transition and the transition time was studied [9]. The appellation of the “sneak”

transition (the phenomenon preceding the actual transition) was given in [9] but this phenomenon was previously characterized in [9] experimentally and in [10] numerically.

The transition was numerically examined by several teams [11–13] in order to obtain or to investigate the time needed for this transient phenomenon. The Baldwin–Lomax turbulent model was employed in time-accurate computations for this dual-bell transition problem [11]. The predicted transition duration agreed reasonably well with the experiments but the transition started for a minimum pressure ratio of 10% higher than the experimental value. This discrepancy was attributed to compressibility effects not taken into account in the turbulent model [11]. In the numerical study [12] performed in 2005, it was found that the deflection angle at the wall inflection should be larger than the angle determined by a Prandtl–Meyer expansion. Also, it was found in this Japanese study that the time to accomplish the separation point transition from the wall inflection to nozzle extension was less than 10 ms when applied to the booster engine of H-2A launch vehicle. In another Japanese study [13], the flow transition by testing 9 dual-bell nozzles in a cold gas facility was investigated experimentally. "Instantaneous" movement of the separation point was found to occur during transition for nozzle extensions with either positive or zero wall pressure gradient.

3 DESIGN METHOD OF DUAL-BELL NOZZLE CONTOUR

3.1 Pressure Parameters of Dual-Bell Nozzle

The occurrence of the flow regimes will be determined by the values of two wall pressure values p_1 and p_2 at the tip of the base nozzle (or at the junction) and at the tip of the nozzle extension, respectively. Wall pressures p_1 and p_2 have been determined by CNES in order to optimize the payload capability of the PERSEUS nanolauncher. The base mission of the PERSEUS project is the putting of a 10-kilogram payload into polar orbit at altitude of 250 km [14]. This optimization results in the following values: $p_1/p_t = 0.01252$ and $p_2/p_t = 0.00124$.

3.2 Base Nozzle

The base nozzle profile is determined [15] using the inverse method of characteristics if one knows the boundary conditions at the inlet (transonic domain) and on the centerline.

The first step is to fix a curvature radius for the throat geometry, then to calculate with an Euler code the transonic flow in this region (Fig. 3). A second

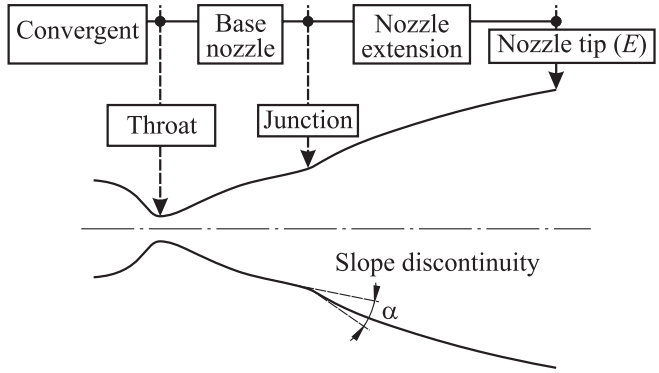

Figure 1 Nomenclature of a dual-bell nozzle

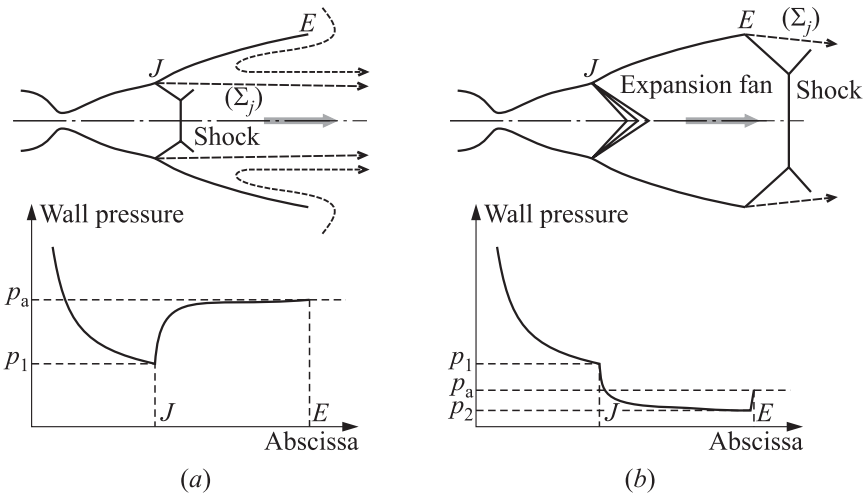

Figure 2 Sea level (a) and altitude (b) modes

wall pressure distribution corresponding to the first flow regime is also given in Fig. 2*a*. The pressure curve is characterized, first, by a decrease due the expansion of the supersonic flow along the wall, then, by a rapid pressure rise induced by the shock to adapt the ambient pressure which is greater than the jet static pressure p_1 at the junction. The nozzle extension is fully separated and external air is entrained into the separation zone at a pressure value p_a.

The altitude mode (Fig. 2*b*) occurs when NPR > NPR_{crit}. The propulsive jet, after expanding at the junction, remains reattached to the wall of the nozzle extension. Immediately after the transition, the jet is overexpanded and sep-

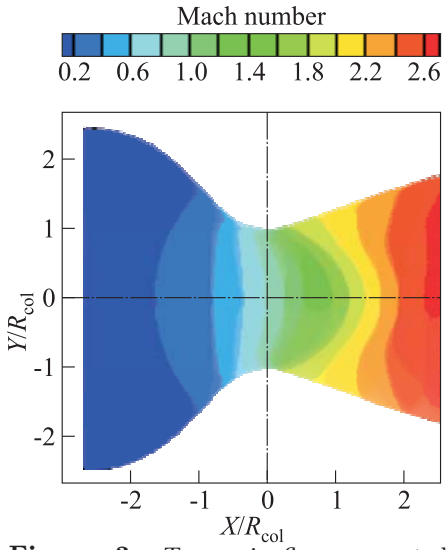

Figure 3 Transonic flow computed by an Euler code. (Refer Reijasse *et al.*, p. 660.)

step is to fix the boundary conditions for the next computation by the method of characteristics. The first boundary condition comes from the extraction of a starting characteristic line from the supersonic domain formerly computed. The second boundary condition is obtained by the building of pressure polynomial curve on the centerline. The pressure polynomial curve has to respect two values: one at the end of the transonic domain (point 00 in Fig. 4) and another at the point which starts the constant Mach number zone. The third step is to calculate the characteristic mesh point-by-point and to extract the fluid perfect streamline issuing from a series of points P_i respecting the throat mass flow rate. The last step is the Euler computation of the whole ideal nozzle; the Euler computation can be compared with the method of characteristics (Fig. 5).

The base nozzle is obtained by truncating the ideal nozzle at the wall abscissa where the pressure value p_1 is found. This corresponds to the exit Mach number $M_1 = 3.53$ at the wall of the truncated ideal nozzle. The two parameters for studying the ideal nozzle are the design Mach number M_{id} and the length of the ideal nozzle L_{id} issued from the length of the centerline pressure law. The range of design Mach number M_{id} studied was from 3.6 to 3.9; the maximum value studied $M_{id} = 3.9$ gives the best specific impulse. The Mach number M_{id} was

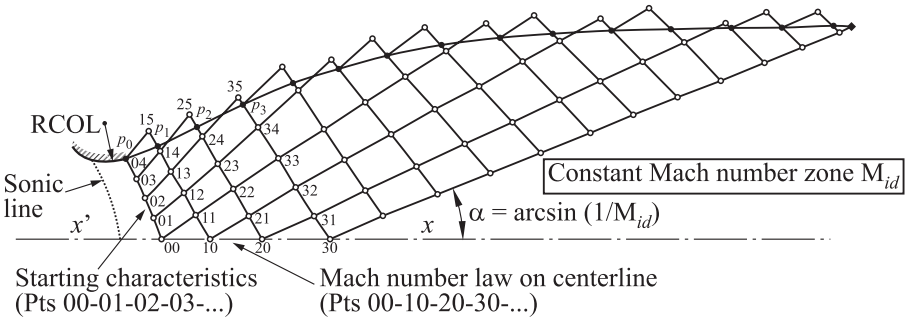

Figure 4 The inverse method of characteristics for the base nozzle contour

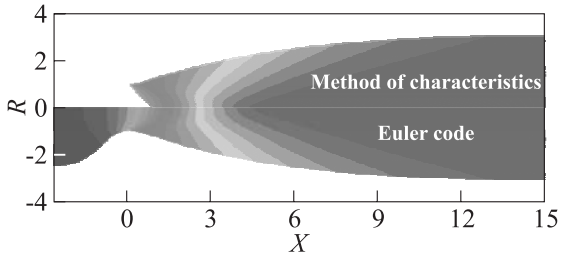

Figure 5 Plot of Mach number contour in the base nozzle; method of characteristics (top) and Euler code (bottom)

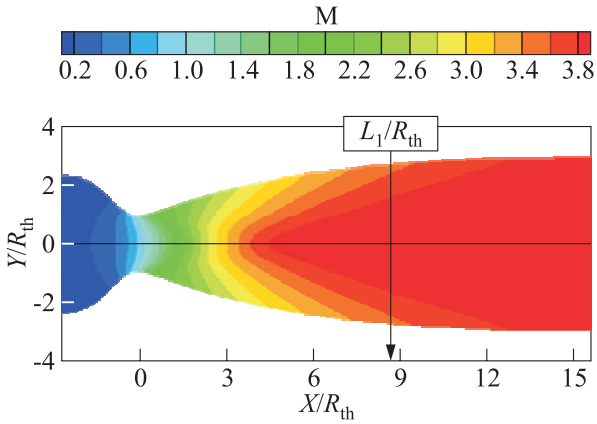

Figure 6 Base nozzle obtained by truncation of the ideal nozzle at $L_1/R_{th} = 8.833$. (Refer Reijasse *et al.*, p. 661.)

limited to 3.9 because of the limitation of the nozzle exit radius. Finally, one retains the ideal nozzle giving a design Mach number of 3.9. This ideal nozzle has been truncated at $L_1/R_{th} = 8.833$ (Fig. 6) in order to reach the exit pressure p_1 at the wall. Table 1 summarizes the base nozzle characteristics.

Table 1 Summarized characteristics of the base nozzle

Parameters	Ideal nozzle	Base nozzle
Isentropic pressure ratio at the exit, p_1/p_t		0.01252
Exit Mach number	3.9	3.533
Normalized specific impulse, I_{sp_1}/I_{sp_throat}	1.294	1.282
Nozzle length, L_1/R_{th}	15.582	8.833
Exit radius, Y_1/R_{th}	3.106	2.879

3.3 Nozzle Extension

The nozzle extension contour is defined to give a constant wall pressure p_2. For an inviscid fluid assumption, this contour is coincident with an isobaric fluid-perfect streamline of pressure p_2. This streamline is obtained with the use of the direct method of characteristics by applying a centered expansion of intensity p_2/p_1 at the junction (Fig. 7). The computed iso-Mach number contour map is given in Fig. 8.

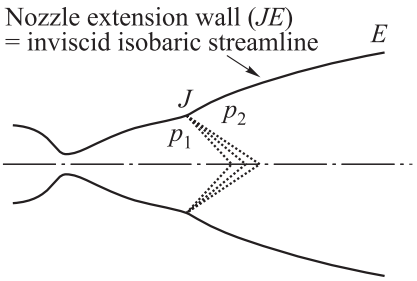

Figure 7 Centered expansion at junction J

For mechanical reasons, the nozzle extension length L_2 has been limited to twice the base nozzle length. The nozzle extension length L_2 is thus equal to 17.67.

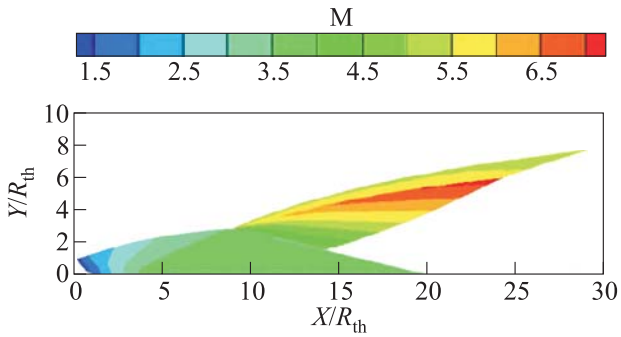

Figure 8 Plot of supersonic Mach-number contour in the dual-bell nozzle calculated with the method of characteristics. (Refer Reijasse *et al.*, p. 662.)

4 EXPERIMENTAL SETUP

Tests have been realized in the blowdown wind tunnel ONERA-R2Ch of Meudon Center. A photograph of the experimental setup is presented in Fig. 9. The nozzle model is fixed on a cylindrical tube which is an interface between the model and the balance. The tube consists of a chamber which is supplied with compressed air by the use of four feeding pipes. The feeding pipes are positioned normal to the thrust axis. Downstream of the nozzle mockup, a supersonic diffuser running as an ejector is installed. In such a configuration, the experimental apparatus runs as an altitude chamber.

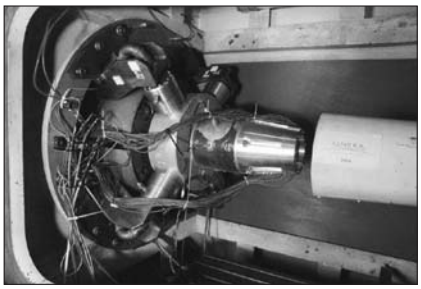

Figure 9 Dual-bell nozzle model in the ONERA R2Ch test chamber

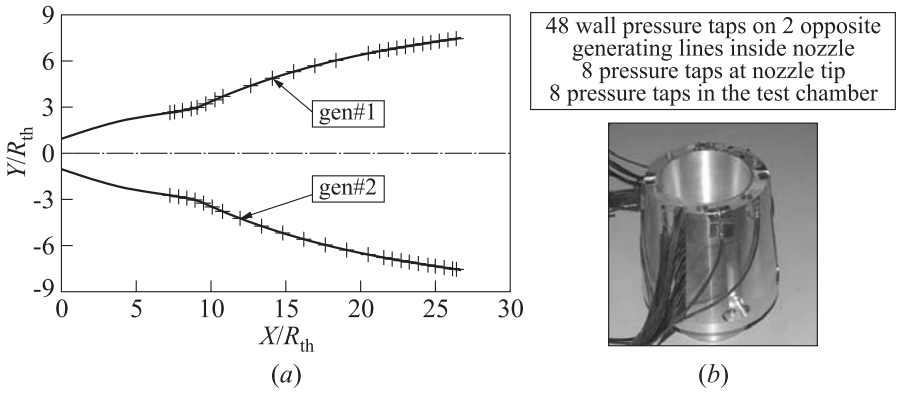

Figure 10 Internal dual-bell contour (a) and wall pressure tap positions (b)

Normalized by the throat radius, the convergent part of the nozzle model is $5.68R_{\text{th}}$ long, and the dual-bell diverging part is $26.51R_{\text{th}}$ long. The exit diameter is $14.92R_{\text{th}}$. Forty-eight pressure taps are distributed on two generating opposite lines named gen#1 and gen#2 (Fig. 10).

The forces and torques have been measured with a 6-component wall balance containing three axial dynamometers and three transverse dynamometers.

5 TEST RESULTS

5.1 Nozzle Pressure Ratio Stabilization

The objective of this test campaign was to characterize the wall pressure distributions and the axial thrust of the dual-bell nozzle model at different NPR in

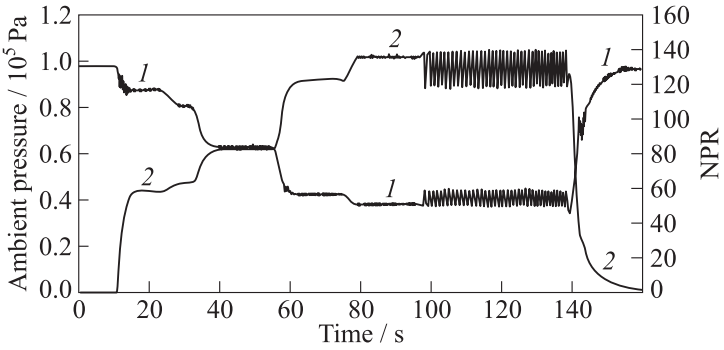

Figure 11 Time histories of ambient pressure (*1*) and NPR (*2*) (test with increasing NPR)

steady regime. The total pressure of the nozzle jet was constant and fixed to $p_t \approx 52 \cdot 10^5$ Pa.

The variation of NPR was obtained by the variation of the ambient pressure p_a in the test chamber. Three combined ways were used to induce the variation of p_a. The first one is to change the geometry of the supersonic ejector (diameter, cone angle, and distance from the nozzle exit), the second one is to manage an entering mass flow rate into the test chamber through an opening

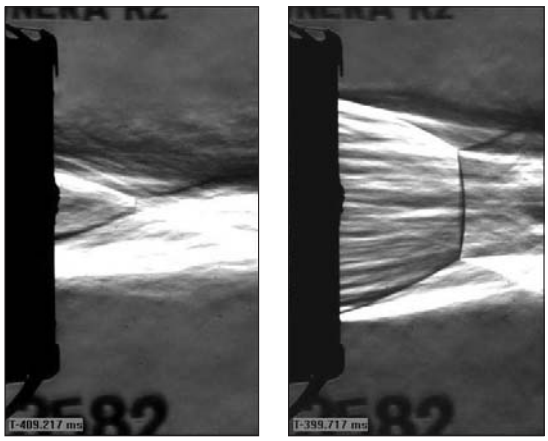

(*a*) (*b*)

Figure 12 Switch of the sea-level mode (*a*) to altitude mode (*b*) at about NPR = 130 (duration of switch is less than 10 ms)

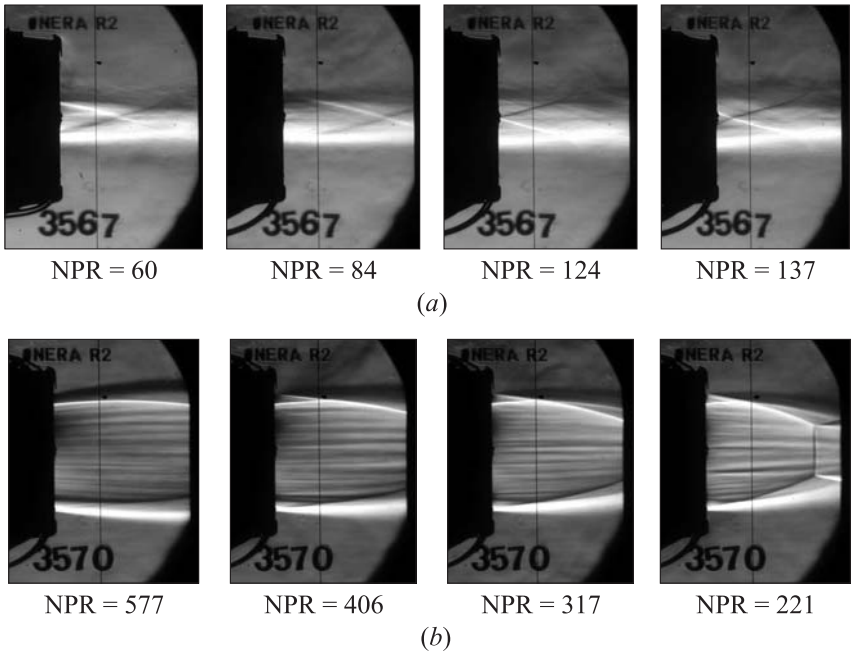

Figure 13 Series of Schlieren photographs of the dual-bell nozzle jet; sea level mode with NPR increasing (a) and altitude mode with NPR decreasing (b)

controlled by a valve, and the last one is to vary the initial pressure value in the test chamber.

With these methods, it was possible to stabilize the lowest values of NPRs in the range $50 < \text{NPR} < 130$ (see, for instance, Fig. 11). For NPRs > 130, it was not possible to perfectly stabilize them even with the smallest ejector diameter tested (Fig. 12).

A series of Schlieren photographs of the dual-bell nozzle jet for the two flow regimes is shown in Fig. 13.

When NPR increases and approaches the value of 140, a phenomenon inducing periodic oscillations of the ambient pressure appears (see Fig. 11). At first, one can see weak oscillations at NPR = 137 for $t < 95$ s. At this NPR, wall pressure signals immediately after the junction were also characterized by strong amplitude oscillations. The first regime of oscillations can be attributed to the beginning of a sneak transition as mentioned in [9]. The second regime of oscillations, with a bigger amplitude between NPR = 120 and 140, is observed for $t > 95$ s; the apparent frequency is about 1 Hz. This range of NPR oscillations corresponds to the switch domain range from the sea level mode to altitude

mode. This oscillation frequency is apparent because it is given by steady pressure taps. In fact, the switch phenomenon is much more rapid than 1 Hz; it occurs in a duration time less than 10 ms as it has been observed at Schlieren photographs (see Fig. 13). One can also notice that the first oscillation begins at the highest value NPR=140 (see Fig. 11).

For decreasing NPR, the same type of oscillations has been observed when NPR approaches the switch domain. One has to keep in mind that these high-amplitude oscillations are a parasitic phenomenon due to the combination of two facts: the coupling between the test chamber pressure and the dual-bell transition and the slow evolution of NPR. In case of rapid NPR evolution, no oscillation was registered.

5.2 Vacuum Pressure Profiles

The dual-bell contour has been determined using an inviscid method. No boundary layer correction has been made for the wall. One can see (Fig. 14) that the wall pressure distributions obtained by the method of characteristics (solid curve) and computed by the RANS code (dashed curves); these computations can be compared with the experimental data for the highest NPR tested (NPR = 435). Some discrepancies appear for the method of characteristics around the junction; this is due to the fact that the inviscid method uses a centered expansion at the junction while the real flow develops a boundary layer which smoothens the geometrical singularity. Another small difference appears for both computations as they cannot reproduce a slight augmentation of the measured wall pressure on the nozzle extension near the extremity. The measured pressure value is $\overline{p}_2 = 0.00164$ instead of 0.00124 predicted by the Euler method. This overpressure can be due to a beginning of air condensation knowing that the nozzle jet Mach number is $M_2 = 5.34$ and that the total temperature is about 330 K.

5.3 Wall Pressure Profiles Around Mode Transition

The adaptation of the base nozzle during the sea-level mode is obtained at NPR = 80. At NPR > 80, one can see (Fig. 14) that the flow expands at the junction just before crossing a separation shock. The fact that the flow separates not at, but downstream of the wall inflection is referred in [8] to as "sneak transition."

For ground conditions, the atmospheric pressure being 1 bar, the nozzle pressure ratio will be NPR = 50 (see dashed line in blue, Fig. 14); the base nozzle will run in slightly overexpanded flow regime. Nevertheless, this overexpansion regime will not induce an extended flow separation (i.e., with external recirculating air inside the base nozzle) because full-flowing of the base nozzle is reached

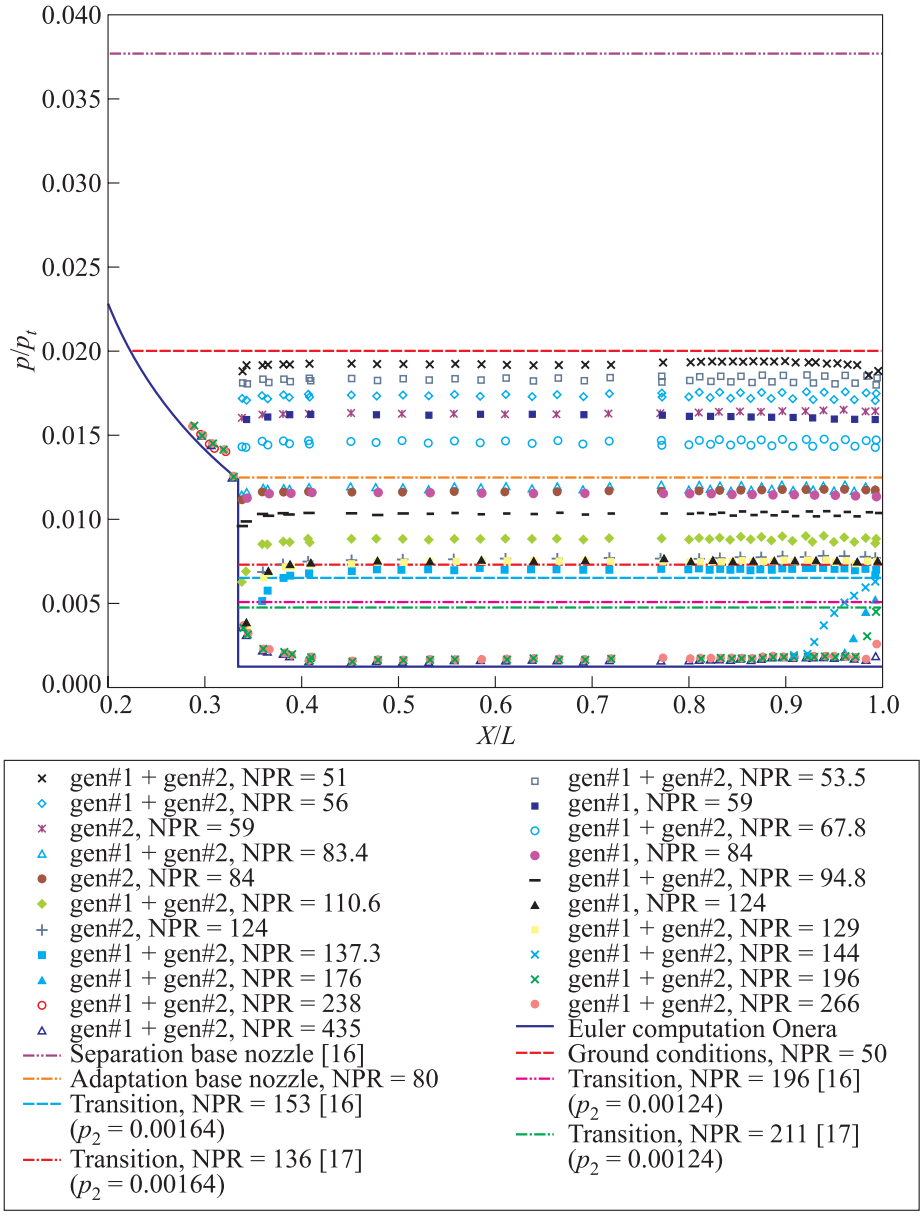

Figure 14 Wall pressure profiles vs. NPR. (Refer Reijasse *et al.*, p. 667.)

already at NPR = 26 according to the Schmucker criterion [16] (see dashed line in rose, Fig. 14).

The mode transition occurs in the NPR range from 138 up to 144 according to the experiments. A method to estimate the transition NPR while NPR is increasing ($\mathrm{NPR}_{\mathrm{tr,inc}}$) is to assume that, immediately after the transition, the nozzle extension flow is overexpanded with an incipient separation at the nozzle extremity. Let consider two supersonic flow separation criteria:

(1) the Schmucker criterion, $p_{\mathrm{a}}/p_2 = (1.88\mathrm{M}_2 - 1)^{0,64}$ where p_2 is the vacuum wall pressure on the nozzle extension; and

(2) the Schilling criterion [17], $p_2/p_{\mathrm{t}} = 0.582(p_{\mathrm{t}}/p_S)^{-1,195}$ where p_S is the pressure in the separated region, not too far from the external or ambient pressure, and p_{t} is the total pressure.

With the pressure value predicted by the inviscid method $p_2 = 0.00124$, the Schmucker criterion and the Schilling criterion give the following NPR transition values, $\mathrm{NPR}_{\mathrm{tr,inc}} = 196$ and 211, respectively; these $\mathrm{NPR}_{\mathrm{tr}}$ values are higher the experimental ones. In other words, the transition is predicted too late (see dashed lines in red and green, Fig. 14). If one considers the measured value of the wall pressure p_2 ($p_2 = 0.00164$), one finds predicted transition at NPR values closer to the experimental ones, $\mathrm{NPR}_{\mathrm{tr,inc}} = 153$ and 136, respectively (see dashed lines in blue and brown, Fig. 14).

5.4 Thrust

5.4.1 Sea-level mode

The intrinsic thrust is the thrust which does not take into account the contribution issued from external or ambient pressure. The intrinsic thrust $F_{\mathrm{int},1}$ of the base nozzle is computed by the use of an axisymmetric Euler code; the intrinsic thrust normalized by the thrust value at the throat F_{th} is equal to $\overline{F}_{\mathrm{int},1} = F_{\mathrm{int},1}/F_{\mathrm{th}} = 1.282$. The thrust at the throat F_{th} is deduced from the isentropic relation with a Mach number equal to 1. The real thrust $F_{\mathrm{real},1}$ during the sea-level mode is obtained by the relation $F_{\mathrm{real},1} = F_{\mathrm{int},1} - (p_i/\mathrm{NPR})A_{S1}$ where A_{S1} is the exit section of the base nozzle. The thrust evolution of the sea-level mode vs. NPR is plotted in Fig. 15*a*.

5.4.2 Altitude mode

The intrinsic thrust $F_{\mathrm{int},2}$ provided by the nozzle extension alone has been evaluated by the method of characteristics. It was found that $\overline{F}_{\mathrm{int},2} = F_{\mathrm{int},2}/F_{\mathrm{th}}$

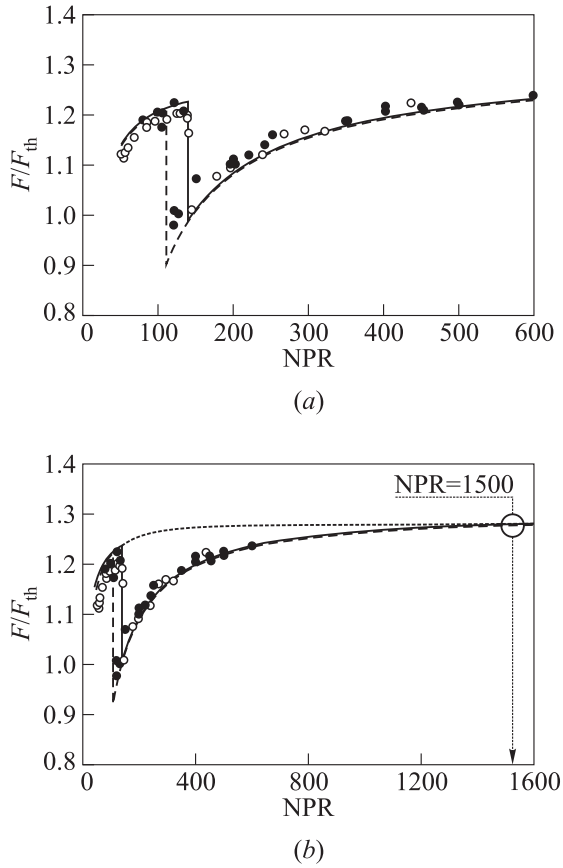

Figure 15 Normalized thrust vs. NPR. Increasing NPR — solid curves and filled signs, decreasing NPR — dashed curves and empty signs: (*a*) hysteresis modeling with the use of supersonic separation criteria (typical loss of thrust after transition of the nozzle extension due to jet induction effect resulting into a pressure p_2 less than the ambient pressure p_a); and (*b*) recovery of the base nozzle thrust at NPR = 1500 (loss of thrust from NPR = 140 up to 1500 comparatively to an isolated base nozzle (dotted line))

= 0.0242. The total intrinsic thrust $\overline{F}_{\text{int,DB}}$ normalized by F_{th} is thus equal to $\overline{F}_{\text{int,DB}} = \overline{F}_{\text{int,1}} + \overline{F}_{\text{int,2}} = 1.3062$. So, the total real thrust of the dual-bell nozzle as a function of NPR is equal to $F_{\text{real,DB}} = F_{\text{int,DB}} - (p_i/\text{NPR})A_{S2}$ where A_{S2} is the exit section of the nozzle extension. The thrust evolution of regime No. 2 vs. NPR is plotted in Fig. 15*a*.

5.4.3 Transition

The transition from the sea-level mode to altitude mode while NPR is increasing, occurs at $\mathrm{NPR}_{\mathrm{tr,inc}} = 136$ for the Schilling criterion and at $\mathrm{NPR}_{\mathrm{tr,inc}} = 153$ for the Schmucker criterion. The transition given by the Schilling criterion is plotted in Fig. 15*a* (solid curve) which is in good agreement with measurements. For decreasing NPR, the measurements give a transition from the altitude mode to sea-level mode at a NPR value between 120 and 104.

Wall pressure profiles before and after the two mode transitions (increasing NPR and decreasing NPR) are plotted in Fig. 16. The shape differences of the wall pressure distributions at the end of the nozzle for the two types of transition are well seen. Immediately after the transition while NPR is increasing, the flow at the extremity of the nozzle extension is in overexpansion regime with an incipient separation (*6*). Just before the transition while NPR is decreasing, the boundary layer resists to the adverse pressure gradient up to the creation of an effective separation with the onset of a plateau pressure (*4*).

The pressure gradient difference between an incipient and effective separation can be expressed with the use of separation criteria issued from the study performed by Zukoski [18] on the supersonic separation properties. The separation criteria are:

– incipient separation criterion: $p_S/p_2 = 1 + 0,73\mathrm{M}_2/2$; and

– effective separation criterion: $p_P/p_2 = 1 + \mathrm{M}_2/2$.

In this study, Mach number M_2 is equal to 5.34. This gives a 25 percent stronger intensity of the pressure gradient for the transition when NPR is de-

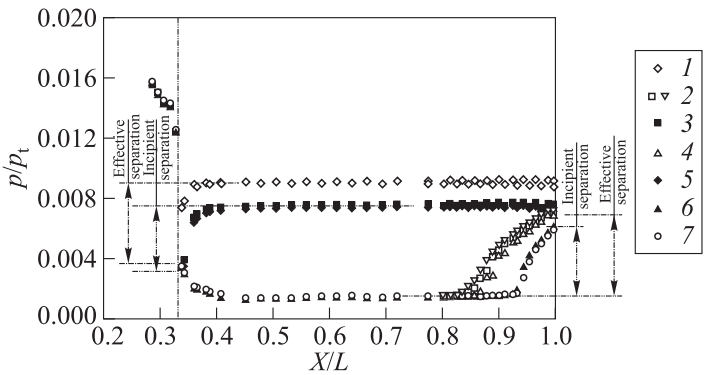

Figure 16 Hysteresis effect on the wall pressure at the extremity of the nozzle extension; NPR increasing (solid symbols); NPR decreasing (empty symbols): *1* — NPR = 104; *2* — 120; *3* — 124; *4* — 126; *5* — 128; *6* — 144; and *7* — NPR = 150

creasing. This corresponds to a transition value $\mathrm{NPR}_{\mathrm{tr,dec}}$ 20% less strong than the $\mathrm{NPR}_{\mathrm{tr,inc}}$. So, the values of NPR transition while NPR is decreasing are: $\mathrm{NPR}_{\mathrm{tr,dec}} = 108$ [17] and $\mathrm{NPR}_{\mathrm{tr,dec}} = 122$ [16]. The NPR transition values deduced from the Schilling's criterion are plotted in Fig. 15*a*.

Figure 15*b* shows that the transition regime induces a loss of thrust up to NPR = 1500 compared to the thrust which should be given by an isolated base nozzle thrust.

6 REYNOLDS-AVERAGED NAVIER–STOKES COMPUTATIONS

First steady Navier–Stokes axisymmetric computations have been done by ENSAM-SINUMEF laboratory [19] with Fluent code at NPR = 400. The turbulence model was the k–ω SST model. The computational domain was $8L_{\mathrm{DB}}$ long and $4.5L_{\mathrm{DB}}$ wide. Three grids were used (X1 mesh: 120 000 cells; X4 mesh: 500 000 cells, and X16 mesh: 2 million cells). The grid convergence was obtained for X4 and X16 grids. The smallest values of Y^+ were 35 for X4 grid and 16 for X16 grid. The computed wall pressure profile is shown in Fig. 17. One can see a good rebuilding of the wall pressure. The Mach disk pattern has been obtained only for X4 and X16 meshes (Fig. 18). One can notice that the Mach disk pattern was visualized at NPR = 221 in Fig. 13. Further steady and unsteady computations are planned, in particular around the transition NPR.

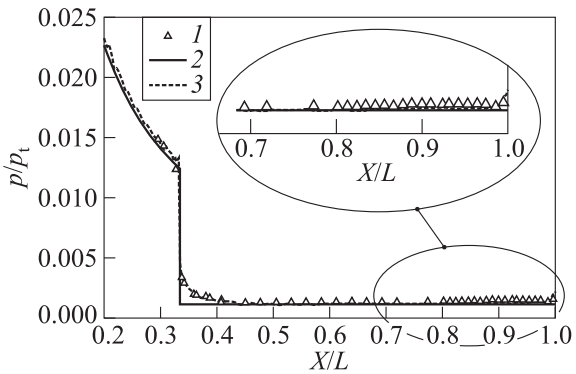

Figure 17 Wall pressure profile: *1* — NPR = 435, Fluent code; *2* — method of characteristics; and *3* — RANS k–ω computation

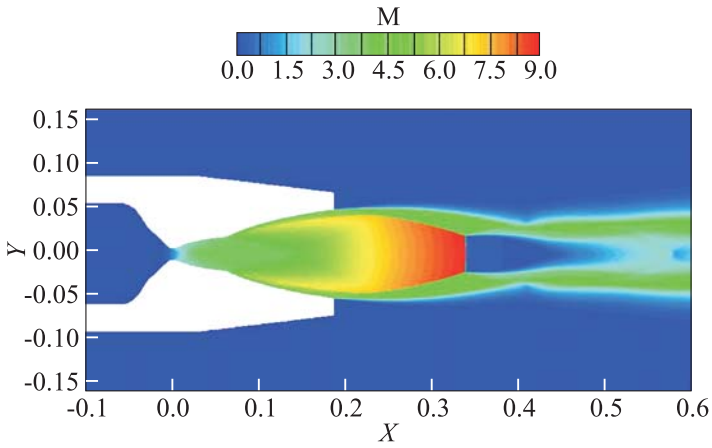

Figure 18 Mach number isocontour plot; NPR = 400; Fluent code. (Refer Reijasse *et al.*, p. 672.)

7 CONCLUDING REMARKS

The test campaign realized in the ONERA-R2Ch wind tunnel has been used to analyze the aerodynamic behavior of a dual-bell nozzle subscale model. The wall pressure distributions for the two flow regimes have been characterized in the NPR range from 51 up to 597. A hysteresis on the transition NPR between the two flow regimes has been observed according to the evolution of NPR.

The transition occurs at about NPR = 140 while NPR is increasing, and at about NPR = 120 while NPR is decreasing. The duration for the switch between the two flow regimes is less than 10 ms.

The wall pressure values predicted by the Euler method are in good agreement with the measured pressure data. Nevertheless, small discrepancies appear at the junction because the modeling with the use of a centered Prandtl–Meyer expansion does not reproduce the viscous phenomena of the boundary layer which smoothens the geometrical singularity. Another small difference appears with the wall pressure level on the nozzle extension; the overestimation of the fluid perfect wall pressure in the final part of the nozzle can be due to the beginning of air liquefaction as the Mach number is 5.34 and the total temperature is about 330 K.

An estimation of the nozzle thrust has been made with the Euler method. The thrust values are normalized by the thrust produced at the throat region. The hysteresis of about 20% on the NPR is also directly applied to the thrust. The total thrust of the dual-bell nozzle becomes higher than the base nozzle thrust for NPR > 1500.

Transition NPR can be modeled by the use of separation criteria which have to take into account that incipient separation occurs immediately after the transition for increasing NPR, while effective separation occurs just before the transition for decreasing NPR. However, this simple modeling does not give a physical explanation of the hysteresis which is governed by viscous effects.

REFERENCES

1. Bec, R., C. Bernard-Lepine, K. de Groote, and F. Amouroux. 2007. PERSEUS. A nanosatellite launch system project focusing on innovation and education. *2nd EUropean Conference for AeroSpace Sciences (EUCASS)*. Liège (BE).
2. Foster, C., and F. Cowles. 1949. Experimental study of gas-flow separation in overexpanded exhaust nozzles for rocket motors. ORDCIT Project, Progress report No. 4-103. Pasadena, CA.
3. JAXA/Kakuda Space Center. 2003. Combustor and nozzle section. http://www.rocket.jaxa.jp/kspc/english/reserch/functional.html.
4. Haas, L. 2002. Liquid rocket engine nozzles. Boeing/Rocketdyne P&P. Presentation to UCLA class.
5. Stephan, B., A. Beaurain, M. Pons, D. Preclick, A. I. Pettersson, and M. Gruslin. 2002. Technology demonstrators for VULCAIN 3 engine. *6th Symposium (International) on Propulsion for Space Transportation of the XXI Century Proceedings*. Versailles, France.
6. Horn, M., and S. Fisher. 1994. Dual-bell altitude compenstaing nozzles. NASACR-194719.
7. Frey, M., and G. Hagemann. 1999. Critical assessment of dual-bell nozzles. *J. Propul. Power* 15(1).
8. Hagemann, G., M. Terhardt, D. Haeseler, and M. Frey. 2002. Experimental and analytical design verification of the dual-bell Concept. *J. Propul. Power* 18(1).
9. Nürnberger-Genin, C., and R. Stark 2008. Flow transition in dual bell nozzles. *Shock Waves J.* 19(3):265–70.
10. Nasuti, F., and M. Onofri. 2001. Flow analysis and methods of design for dual-bell nozzles. AIAA Paper No. 2001-3558.
11. Wong, H., and R. Schwane. 2001. Numerical investigation of transition in flow separation in a dual-bell nozzle. *4th European Symposium on Aerothermodyanmics for Space Applications Proceedings*. Capua, Italy. ESA SP-487, 2002.
12. Otsu, H., M. Miyazawa, and Y. Nagata. 2005. Design criterion of the dual-bell nozzle contour. IAC-05-C4.2.08.
13. Tomita, T., M. Takahashi, M. Sasaki, and H. Tamura. 2006. Investigation on characteristics of conventional-nozzle-based altitude compensating nozzles by cold-flow tests. AIAA Paper No. 2006-4375.
14. www.cnes.fr/perseus.

15. Reijasse, P. 2009. Conception d'un profil de tuyère double-galbe. Programme PERSEUS. [In English: Design of a dual bell nozzle contour. PERSEUS program. Under CNES contract. Report ONERA RT 1/14512 DAFE.]
16. Schmucker, R. 1974. Status of flow separation prediction in liquid propellant rocket nozzle. NASA TM X-64890.
17. Schilling, M. 1962. Flow separation in a rocket nozzle. M.S. Thesis. University of Buffalo.
18. Zukoski, E. 1967. Turbulent boundary layer separation in front of a forward-facing step. *AIAA J.* 5(10).
19. Kuszla, P. 2009. Preliminary dual bell nozzle RANS computations at NPR = 400. PERSEUS technical meeting presentation, ENSAM-SINUMEF.